AIP Journal of Applied Physics

Nonlinear photoresponse of field effect transistors terahertz detectors at high irradiation intensities

D. B. But, C. Drexler, M. V. Sakhno, N. Dyakonova, O. Drachenko, F. F. Sizov, A. Gutin, S. D. Ganichev, and W. Knap

Citation: Journal of Applied Physics **115**, 164514 (2014); doi: 10.1063/1.4872031
View online: http://dx.doi.org/10.1063/1.4872031
View Table of Contents: http://scitation.aip.org/content/aip/journal/jap/115/16?ver=pdfcov
Published by the AIP Publishing

Articles you may be interested in
Ultrahigh sensitive sub-terahertz detection by InP-based asymmetric dual-grating-gate high-electron-mobility transistors and their broadband characteristics
Appl. Phys. Lett. **104**, 251114 (2014); 10.1063/1.4885499

Plasmonic terahertz detector response at high intensities
J. Appl. Phys. **112**, 014508 (2012); 10.1063/1.4732138

Helicity sensitive terahertz radiation detection by field effect transistors
J. Appl. Phys. **111**, 124504 (2012); 10.1063/1.4729043

High-responsivity, low-noise, room-temperature, self-mixing terahertz detector realized using floating antennas on a GaN-based field-effect transistor
Appl. Phys. Lett. **100**, 013506 (2012); 10.1063/1.3673617

Terahertz response of field-effect transistors in saturation regime
Appl. Phys. Lett. **98**, 243505 (2011); 10.1063/1.3584137

AIP Journal of Applied Physics

Journal of Applied Physics is pleased to announce André Anders as its new Editor-in-Chief

[This article is copyrighted as indicated in the article. Reuse of AIP content is subject to the terms at: http://scitation.aip.org/termsconditions. Downloaded to] IP: 132.199.96.80 On: Fri, 25 Jul 2014 05:14:38

JOURNAL OF APPLIED PHYSICS **115**, 164514 (2014)

Nonlinear photoresponse of field effect transistors terahertz detectors at high irradiation intensities

D. B. But,[1,2] C. Drexler,[3] M. V. Sakhno,[2] N. Dyakonova,[1] O. Drachenko,[4] F. F. Sizov,[2] A. Gutin,[5] S. D. Ganichev,[3] and W. Knap[1,6]
[1]*UMR 5221 CNRS, Université Montpellier 2, Montpellier 34095, France*
[2]*V. E. Lashkaryov Institute of Semiconductor Physics, National Academy of Sciences of Ukraine, Kiev, 03028, Ukraine*
[3]*Terahertz Center, University of Regensburg, Regensburg 93040, Germany*
[4]*Helmholtz Zentrum Dresden Rossendorf, Institute of Ion Beam Physics and Materials Research, Dresden 01314, Germany*
[5]*Rensselaer Polytechnic Institute, Troy, New York 12180, USA*
[6]*Institute of High Pressure Physics, Polish Academy of Sciences, Warsaw 02845, Poland*

(Received 3 February 2014; accepted 9 April 2014; published online 30 April 2014)

Terahertz power dependence of the photoresponse of field effect transistors, operating at frequencies from 0.1 to 3 THz for incident radiation power density up to 100 kW/cm^2 was studied for Si metal–oxide–semiconductor field-effect transistors and InGaAs high electron mobility transistors. The photoresponse increased linearly with increasing radiation intensity up to the kW/cm^2 range. Nonlinearity followed by saturation of the photoresponse was observed for all investigated field effect transistors for intensities above several kW/cm^2. The observed photoresponse nonlinearity is explained by nonlinearity and saturation of the transistor channel current. A theoretical model of terahertz field effect transistor photoresponse at high intensity was developed. The model explains quantitative experimental data both in linear and nonlinear regions. Our results show that dynamic range of field effect transistors is very high and can extend over more than six orders of magnitudes of power densities (from ~0.5 mW/cm^2 to ~5 kW/cm^2).
© *2014 AIP Publishing LLC*. [http://dx.doi.org/10.1063/1.4872031]

I. INTRODUCTION

Electromagnetic waves in the terahertz (THz) frequency range are gaining importance because of many applications in the domains of security, biology, imaging, material control, and characterization. The development of many of these applications is hindered by the lack of sensitive and robust room temperature detectors, especially with high dynamic range. The THz detection phenomenon in field-effect transistors (FETs) was explained by the Dyakonov-Shur plasma wave theory.[1] When THz radiation is coupled to the FET—between gate and source—the THz *ac* voltage modulates simultaneously carrier density and the carrier drift velocity. As a result, THz *ac* signal is rectified and leads to a *dc* photoresponse between source and drain proportional to the received power. For high carrier mobility devices (III–V devices at cryogenic temperatures), the THz field can induce plasma waves that propagate in the channel and resonant plasma modes can be excited leading to weak voltage tunable detection.[2,3] At room temperature, plasma waves are overdamped and THz radiation leads only to a density perturbation that decays exponentially with the distance from the source with the characteristic length L_{eff} that is typically on the order of a few tens of nanometers.[4] A more detailed description of the physical mechanism of THz detection by FETs can be found in Ref. 5. In the case of room temperature, broadband detection the detection process can be alternatively explained by the model of distributed resistive self-mixing.[6,7] Although not treating all plasma related physics rigorously, the resistive mixing model allows a rational detector design.[7,8] THz FET detectors show high responsivity (up to a few kV/W), low noise equivalent power (down to 10 pW/$\sqrt{\text{Hz}}$),[9] and fast response time (below 1 ns (Ref. 10) and 30 ps (Ref. 11)). Additional interesting properties of the FET detector were recently discovered, where the photoresponse exhibits sensitivity to radiation helicity[10,12] making FETs promising for the all-electric detection of the radiation Stokes parameters. However, there have been very few studies of THz FET detectors at high radiation intensities. The first high intensity experiments were reported in Ref. 13. It was shown that for GaAs high electron mobility transistors (HEMTs), the photoresponse remained linear in radiation intensity up to 8 ± 4 kW/cm^2 (11 W total intensity) at 240 GHz, followed by a non-linear photoresponse. For moderate intensity (up to 0.5 kW/cm^2 at 1.63 THz), the broadband detection by FETs versus the radiation power was studied in Ref. 14, where a linear power dependence, followed by a square root dependence for higher intensities was observed.

Here, we report the radiation intensity dependent photoresponse of FETs in a very wide intensity range going up to 500 kW/cm^2. We demonstrate that for InGaAs HEMTs and silicon metal–oxide–semiconductor field-effect transistors (Si-MOSFETs), there are a large interval of linear dependence followed by non-linear dependence and saturation. We have developed a model describing the FET photoresponse in a wide range of intensities. It allows quantitative data interpretation using parameters determined from direct currents (*dc*) output characteristics. The saturation is explained

[This article is copyrighted as indicated in the article. Reuse of AIP content is subject to the terms at: http://scitation.aip.org/termsconditions. Downloaded to] IP: 132.199.96.80 On: Fri, 25 Jul 2014 05:14:38

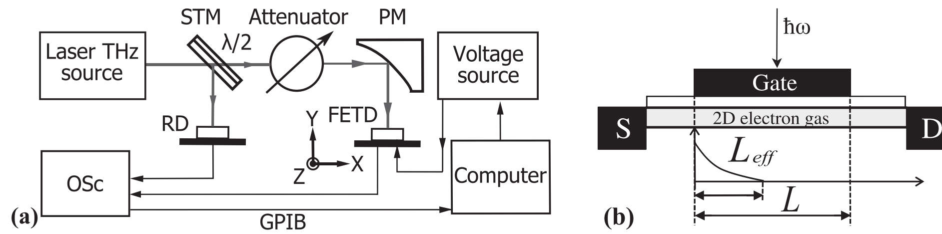

FIG. 1. (a) Schematic illustration of experimental setup. STM is a semitransparent mirror, PM is a parabolic mirror, OSc is an oscilloscope, RD is a reference detector, FETD is THz FET detector. (b) Schematic view of the HEMT device with contact terminals S (source), D (drain), and G (gate). Transistors were irradiated by linearly polarized radiation at normal incidence in all optical experiments. L and L_{eff} are length and effective detection length of transistor channel, respectively.

by analogy with the standard *dc* current saturation. The calculated photoresponse shows close agreement with experimental data both in the linear and nonlinear regions. Our experimental results show that the dynamic range of FETs based detectors is relatively high and can extend over a wide range of intensities from ~0.5 mW/cm^2 to ~5 kW/cm^2.

II. EXPERIMENTAL

To study the room temperature detector responsivity in a wide intensity range from 0.5 mW/cm^2 to 500 kW/cm^2, we used several types of monochromatic continuous wave (*cw*) and pulsed sources operating in the frequency range from 0.13 THz to 3.3 THz. In this paper, as a basic parameter we use the peak radiation intensity at the detector location to consistently describe experimental data obtained with different sources and beam waists.

As high intensity sources (>1 W/cm^2), we used an optically pumped molecular terahertz laser of the Regensburg Terahertz Center TerZ[15–17] and the free electron laser at Rossendorf Helmholtz Institute system FELBE.[18] Using NH_3 as the active medium for the molecular laser, we obtained linearly polarized radiation with frequencies 3.33, 2.03, and 1.07 THz. Lower frequencies of 0.78 and 0.61 THz were achieved using D_2O and CH_3F, respectively. The molecular laser generated single pulses with duration of about 100 ns, peak intensity ~500 kW/cm^2, and a repetition rate of 1 Hz. Radiation power was controlled by the THz photon drag detector[19] (Fig. 1(a)). By focusing the laser beam with a parabolic mirror, we achieved an almost Gaussian profile, as recorded with a pyroelectric camera,[20] and exhibiting full widths at half maximum between 1 mm (at 3.33 THz) and 3 mm (at 0.61 THz). To vary the radiation intensity, we used a set of teflon, black polyethylene, and/or pertinax calibrated attenuators.[21] THz FET photoresponses were measured using an oscilloscope. In this set-up, photoresponse was measured as a voltage drop over a 50 Ω load resistor and fed into an amplifier with a bandwidth of 300 MHz and a voltage amplification of 20 dB. The FEL provided 6.22 ps pulses at 1.55 THz and 8.4 ps pulses at 2.11 THz with a repetition rate of 13 MHz and peak intensity ~200 kW/cm^2. The radiation attenuation was achieved using a series of wire grid attenuators. The beam was focused on the sample by a parabolic mirror; the resulting diameter was about 2.5 mm.

Low intensity *cw* radiation (<1 W/cm^2) was obtained using a backward wave oscillator (BWO), a *cw* methanol laser,[15,22] and a commercially available Schottky diode (Radiometer Physics GmbH). The operation frequencies and maximum output power levels were as follows: 129–145 GHz and 15 mW (BWO Γ4-161), 292 GHz and 4.5 mW (Schottky diode source, Radiometer Physics GmbH), 2.54 THz and 20 mW (methanol laser). Radiation from the sources was focused by parabolic mirrors. For BWO and Schottky diode, the beam spatial distribution was monitored during the experiment by a pyroelectric detector (MG-30) and a THz FET with XY-stage at the focal point. The beam had a Gaussian profile with 3–7 mm beam waist depending on radiation source and wavelength. Radiation power was measured by a photo-acoustic power meter (Thomas Keating) and attenuation was controlled by changing source output power directly or by using calibrated attenuators. For the methanol laser, the power and beam spatial distribution were controlled like for high intensity sources.

Detection signals were measured using 50 Ω or 1 MΩ preamplifiers followed by a lock-in amplifier. The peak values of the signal were determined by taking into account the lock-in averaging algorithm with proper frequency and duty factors. When comparing 50 Ω preamplifiers data with other results, all 1 MΩ preamplifiers data were corrected by the load resistance depending factor as described in Sec. IV.

The main parameters of the detectors used in our experiments and the fitting parameters are summarized in Table I. Our experiments were done at room temperature, thus the regime of the detection was broadband (non-resonant). The radiation induced carrier density oscillations decay exponentially along the channel[4] with characteristic length L_{eff} (see Fig. 1(b)).

The HEMT detectors were pseudomorphic based on InGaAs/GaAs structures. The gate length was $L = 0.13\ \mu$m, the gate width W was from 12 to 40 μm, open channel carrier

TABLE I. Sample parameters.

Name	Type	L (μm)	W (μm)	V_{th} (V)	η	μ_n (cm^2/(Vs))	k_{th} (mV/K)	k_μ	A	β	L_{eff} (nm)	k_{ant} cm·(V/W)$^{1/2}$
HEMT	InGaAs	0.13	12–40	−0.18	1.3	2900	0.21	1.6	0.077	0.92	65	212
MOSFET	Si	2	20	0.6	1.75	500	2.1	1.7	0.012	0.9	31	298

[This article is copyrighted as indicated in the article. Reuse of AIP content is subject to the terms at: http://scitation.aip.org/termsconditions. Downloaded to] IP: 132.199.96.80 On: Fri, 25 Jul 2014 05:14:38

mobility was $\mu_n = 2900$ cm^2/(Vs) at $T = 300$ K. Close to the threshold voltage, the mobility was $\mu_n = 1200$ cm^2/(Vs). The mobility was determined by the magneto-resistance technique.[23] The Si MOSFET had $L = 2\,\mu$m and $\mu_n = 500$ cm^2/(Vs). Similar to previous experiments, the bonding wires and metallization of contact pads served as effective antennas.[24,25]

III. RESULTS

Figure 2 shows compilation of the results for different HEMT samples and different types of THz sources. The responsivity R_{VI} is defined as the ratio of detector photoresponse, ΔU, to radiation intensity, $\Im_{ir}$, at the focal point of the parabolic mirror, and is plotted as a function of incident power density. To present the responsivity versus radiation intensity in a way independent of experimental conditions (pulsed, *cw* sources), we consistently used the peak signals and radiation intensity values. The left panel shows R_{VI} for *cw* sources with low output intensity (less than a few mW). The right panel shows R_{VI} for high intensity pulsed sources.

The results could be fitted by the phenomenological formula for determining of the characteristic saturation intensity $\Im_{ir,sat}$,

$$R_{VI}(\Im_{ir}) = R_{VI0}(\Im_{ir})\frac{1}{1+\Im_{ir}/\Im_{ir,sat}}, \tag{1}$$

where $R_{VI0}(\Im_{ir}) = \text{const}$ is the constant responsivity in the linear region ($\Im_{ir} < \Im_{ir,sat}$).

As can be seen in Fig. 2, the responsivity values of THz FETs in pulsed lasers sources are slightly lower than responsivity values in *cw* sources at approximately the same frequency (2.11 THz and 2.54 THz). This difference can be explained by the systematical error of pulsed measurements, most probably related to time resolution limitations of the oscilloscope used in pulsed experiments. This systematical error leads to slight underestimation of R_{VI0}. However, we do not perform any normalization between data obtained using two experimental set-ups. This is because the only important fitting result is $\Im_{ir,sat}$ which is independent of any multiplicative factor on R_{VI0}.

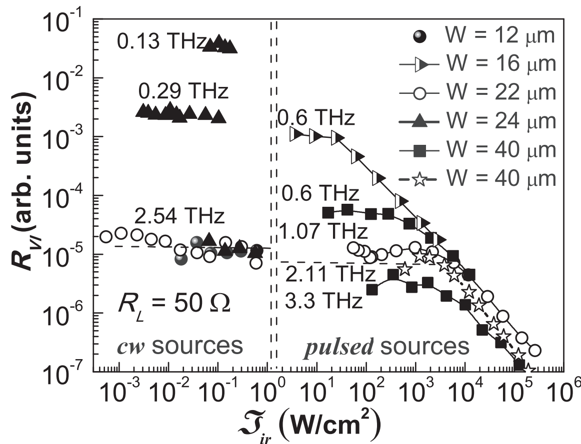

FIG. 2. The responsivity R_{VI} as function of THz radiation intensity $\Im_{ir}$, for several GaAs HEMTs with different gate widths (W = 12, 16, 22, 24, 40 μm) and frequencies. All curves were measured at $V_{GS} = -0.1$ V and $R_L = 50\ \Omega$. Continuous wave (*cw*) sources with frequencies 0.13 THz, 0.29 THz, 2.54 THz results on the left side of the vertical dotted line. Results for laser pulsed sources with frequencies 0.6 THz, 1.07 THz, 3.3 THz and FEL FEBL at 2.11 THz (stars) are shown on the right side. Only high intensity pulsed lasers permitted to observe the non-linear photoresponses of THz FETs (on the right panel).

Figure 2 shows the decreasing dependence of R_{VI0} on the radiation frequency ω (for *pulsed* and *cw* sources). Frequency increase also leads to a shift of the characteristic saturation intensity to higher intensity values. Frequency dependence of photoresponse in the linear region originates from device properties and antenna coupling.[26–28] R_{VI0} for the linear region can be written as

$$R_{VI0}(\omega) = R_{VI0}(\omega_0)\left(\frac{\omega_0}{\omega}\right)^{\gamma}. \tag{2}$$

The influence of FETs parameters and antenna-detector matching on responsivity for low input powers has been analyzed in Ref. 28. In that work, it was assumed that $\gamma = 2$ for matching with lenses and/or wide aperture antennas, and $\gamma = 4$ for other cases.

Figure 3 shows the frequency dependence of R_{VI0}. Measurement data were obtained in the linear region of detector response of pulsed lasers experiments at 10 W/cm^2 (after Fig. 2). The line shows calculations according to Eq. (2) with $\gamma = 2$. This fitting shows close agreement with the responsivity behavior which was proposed in Ref. 28 and verifies experimentally that indeed for matching with lenses and/or wide aperture antennas $\gamma = 2$. This result is also close to the experimental data behavior obtained in Ref. 27.

Figure 4(a) (left ordinate) shows normalized photoresponses (triangles) and fitting lines with a 292 GHz *cw* THz radiation source measured as a function of gate bias V_{GS} at different loading resistances in the linear region of responsivity and a constant radiation frequency. Figure 4(a) shows the same $\Delta U(V_{GS})$ shapes of pulsed (triangles) and *cw* (circles) modes at same load resistance (50 Ω). In both modes, ΔU can be described by the model in Eq. (14a) at constant frequency and constant radiation intensity.

Figure 4(b) shows photoresponse as a function of gate voltage and decreasing response due to temperature T increase for HEMT ($W = 22\,\mu$m) in the linear region of photoresponse. Solid lines in Fig. 4(b) present ΔU fitting using the model

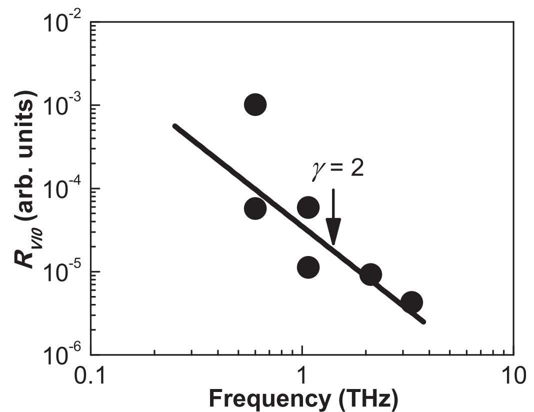

FIG. 3. Responsivity $R_{VI0}(\omega)$ as a function of radiation frequency in the linear region for pulsed detection measurement. Dots are experimental data of FET detectors (sample HEMT) at $\Im_{ir,} = 10$ W/cm^2 (after Fig. 2). Line is fitting of Eq. (2) with $\gamma = 2$.

[This article is copyrighted as indicated in the article. Reuse of AIP content is subject to the terms at: http://scitation.aip.org/termsconditions. Downloaded to] IP: 132.199.96.80 On: Fri, 25 Jul 2014 05:14:38

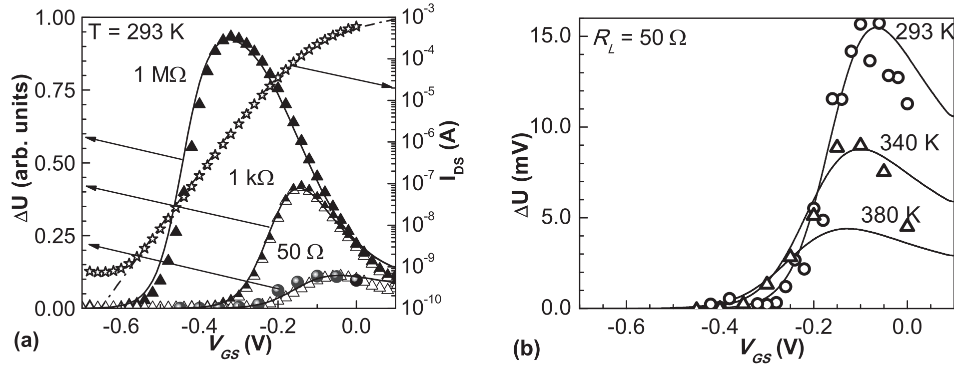

FIG. 4. (a) Left ordinate: photoresponse (the sample HEMT, $W = 22\,\mu$m) as a function of gate bias V_{GS} in linear region of photoresponse at 0.29 THz. Triangles are photoresponses to *cw* THz radiation measured at R_L 1 MΩ, 1 kΩ, and 50 Ω. Full circles are photoresponse to pulsed radiation measured across 50 Ω in linear region of photoresponse at 1.07 THz. Right ordinate: dark drain current as a function of gate bias at drain voltage 50 mV for the HEMT with $W = 22\,\mu$m. Stars are experimental data; dashed-dotted line is fit according to Eq. (17) using parameters of HEMT presented in Table I. (b) Comparison of HEMT ($W = 22\,\mu$m) photoresponses *vs* gate bias at different temperatures in linear region at frequency 1.07 THz (169 W/cm^2): circles and rectangles are experimental data at $T = 293$ K and $T = 340$ K, respectively; solid lines shown fitting results using Eq. (14a) and taking into account the temperature dependence Eqs. (18) and (19) (for parameters k_{th}, k_{μ}, see Table I).

from Eq. (14a), taking into account heating of samples (Eqs. (18) and (19)). The maximum photoresponse shifts to more negative gate voltage ($V_{GS,max} = -0.19$ V at $T = 293$ K and $V_{GS,max} = -0.225$ V at $T = 340$ K) with increasing temperature, and the shape becomes flatter with the maximum value decreasing with temperature rise.

At higher intensities, the photoresponse is no longer linear in radiation intensity. The responsivity R_{VI} decreases in this case (see Fig. 5). Non-linear dependence was demonstrated in experiments[13] on GaAs HEMTs. The linearity of the photoresponse was observed up to 8 ± 4 kW/cm^2 (11 W) on the FEL (UCSB, Santa Barbara) beam power at 240 GHz. In this work, the authors suggested that Si lenses focused 10% to 50% of incident power on the devices. The theoretical model in Ref. 14 provides analytical expressions (for infinite load resistance) for two cases of gate voltage: above and below threshold voltage. In our case when FETs operate above threshold, the theory in Ref. 14 gives

$$\Delta U = \frac{U_a^2}{2(\sqrt{V_0^2 + U_a^2/2} + V_0)}, \quad (3)$$

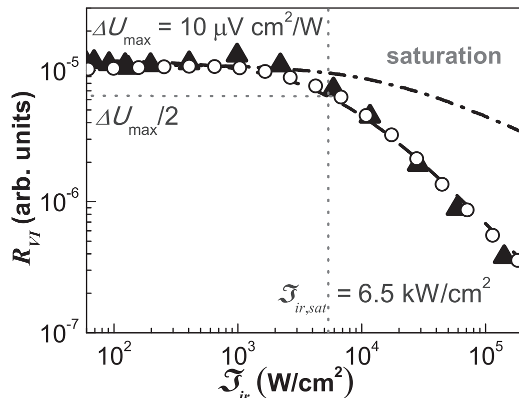

FIG. 5. Responsivity R_{VI} of HEMT sample ($W = 22\,\mu$m) as a function of radiation intensity at frequency 1.07 THz (169 W/cm^2). Full triangles are the experimental data at gate voltage -0.1 V; dashed line is the fit of Eq. (1); dashed-dotted line is fitted using theoretical prediction[14] Eq. (3), empty dots is R_{VI} using the model (Eq. (13)), which takes into account the nonlinear behavior of the channel current in a whole transistor operating range.

where $V_0 = V_{GS} - V_{th}$, V_{th} is the threshold voltage, U_a is the amplitude of the THz signal applied between gate and source.[1]

It was found that at high input radiation intensity ΔU increases not linearly, but as the square root with intensity increase. The experimental results in Ref. 14 were measured at 1.63 THz with power levels varying from 9.5 W/cm^2 to 510 W/cm^2 showing non-linear behavior in agreement with the theory.[14] In this work, at 1.07 THz, we observed the linear dependence up to intensities of ~6.5 kW/cm^2. However, our results (full dots in Fig. 5) show a saturation behavior and cannot be described by the square root dependence proposed by Eq. (3) (the dashed dotted line in Fig. 5). Equation (3) describes only a partial signal *vs* intensity dependence—just after the linear region, most probably due to model assumption of the finite load resistance.

Photoresponses of InGaAs HEMT and Si MOSFET to pulsed radiation are shown in Fig. 6(a). Although the photoresponse magnitude between transistors differ significantly, the dependence of ΔU on the $\Im_{ir}$ is qualitatively the same: at first, it is linear followed by saturation.

The saturation values of photoresponse, ΔU_{sat}, in Fig. 6(a) are 70 mV for HEMT and 3 mV for MOSFET. We convert ΔU_{sat} into the current $\Delta i_{DS,\mathrm{sat}}$ in the measured circuit as $\Delta i_{DS,sat} = \Delta U_{sat}/(R_L + R_{ch})$, where R_L and R_{ch} are the load and the transistor channel resistance, respectively, and obtain 0.7 mA and 30 μA (as shown in the right ordinate axis in Fig. 6(a)). It is important to note that these values are close to saturation currents of non-irradiated devices at the same gate bias as seen in Fig. 6(b). This important observation will be discussed below.

IV. BROADBAND DETECTION MODEL AND DISCUSSION

The antenna of THz FET detectors transforms incoming radiation into voltage V_{ant}. Voltage V_{tr} incident on the detector is given by

$$V_{tr} = \eta_{ant} V_{ant}, \quad (4)$$

[This article is copyrighted as indicated in the article. Reuse of AIP content is subject to the terms at: http://scitation.aip.org/termsconditions. Downloaded to] IP: 132.199.96.80 On: Fri, 25 Jul 2014 05:14:38

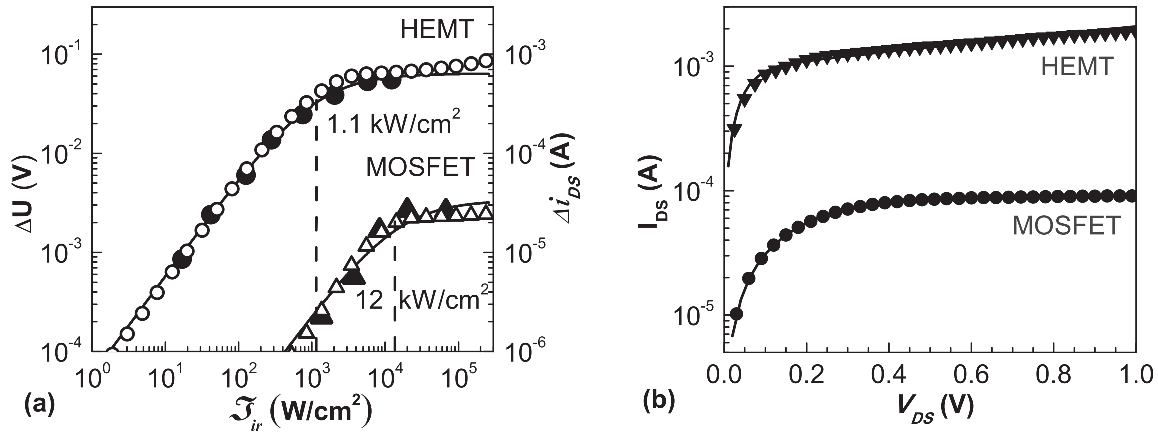

FIG. 6. (a) Photoresponses of HEMT ($W = 40\,\mu$m) and MOSFET (parameters are present in Table I) as a function of radiation intensity at frequency 0.6 THz. The gate voltages are $V_{GS} = -0.1$ V for HEMT and $V_{GS} = -1.4$ V for MOSFET. Full circles and triangles are experimental data of HEMT and MOSFET, respectively. Solid lines are fit according to phenomenological Eq. (1). Full circles and triangles are fitting data points according to model Eq. (13) using parameters of Table I. (b)Output characteristic of HEMT ($W = 40\,\mu$m) and MOSFET samples. Dots and triangles are experimental for gate voltage $V_{GS} = -0.1$ V for HEMT and $V_{GS} = -1.4$ V for MOSFET, respectively. Lines are fit according to Eq. (17) using parameters of Table I.

where η_{ant} is the coefficient representing losses in the parasitic elements and impedance mismatch between antenna and detector. The input impedance is defined by the impedance of the antenna transmission line.

The maximum power, P_{ant}, which is supplied to the FET channel from the antenna, is given by[29]

$$P_{ant} = G\frac{\lambda^2}{4\pi}\Im_{ir}, \tag{5}$$

here, G is the antenna gain coefficient, λ is the wavelength in vacuum. V_{ant} can be rewritten using Eq. (5),

$$V_{ant}^2 = G\frac{2}{\pi}\lambda^2\Im_{ir}\mathrm{Re}Z_{ant}, \tag{6}$$

where Z_{ant} is the antenna impedance.[28]

Taking into account Eq. (6), Eq. (4) can be rewritten as

$$V_{tr} = k_{ant}\sqrt{\Im_{ir}}, \tag{7}$$

where k_{ant} is the fitting parameter which depends on antenna parameters and impedance matching.

The effective rectification length L_{eff} (see Fig. 1(b)) can be approximately calculated as[30]

$$L_{eff} = \sqrt{\frac{\mu_n n}{\omega(dn/dU)|_{U=V_{GS}}}} \approx \sqrt{\frac{\mu_n(V_{GS}-V_{th})}{\omega}}, \tag{8}$$

where n is the electron concentration in channel.

Values of L_{eff} are shown in Table I for 0.6 THz for our experimental samples.

A transistor at THz frequency can be represented by distributed RLC elements.[7,31] Our model is based on the assumption that FETs can be divided into two parts: the first with length L_{eff} where the rectification takes place (see Fig. 1(b)) and the second with length $(L - L_{eff})$ connected in series (see Fig. 7). THz voltage and current are present only in the first part, and the second is considered like as a load. To model such behavior, we add elements L_1, L_2, C_1 to the equivalent circuit. Inductance L_1 models the absence of THz current flow through the load resistor. Inductance L_2 models the absence of THz voltage on the gate of the load part with length $(L - L_{eff})$. Capacitance C_1 is the gate-to-channel capacitance of the load part, and i_c represents the *ac* THz current through the gate. C_g models two sources (V_{GS0}, V_{tr}) decoupling. The v_{GS1} and v_{GS2} is the gate voltage at L_{eff} and $L - L_{eff}$, respectively.

Let us assume that the signal current flows in the circuit formed by the detector and an external load R_L. The v_{DS} is the voltage between source and drain. The v_{DS1} is the voltage drop over characteristic length L_{eff}; and v_{DS2} is the voltage drop on the length $(L - L_{eff})$. Current through part L_{eff} is given by Eq. (17) with corresponding values

$$i_{DS1} = I_{DS}(v_{DS1}, v_{GS1}, L_{eff}), \tag{9}$$

where

$$v_{DS1} = -v_{DS2} - R_L i_L + V_{tr}\cos(\omega t), \tag{10a}$$

$$v_{GS1} = V_{GS0} + V_{tr}\cos(\omega t). \tag{10b}$$

The current through part $(L - L_{eff})$ is given by

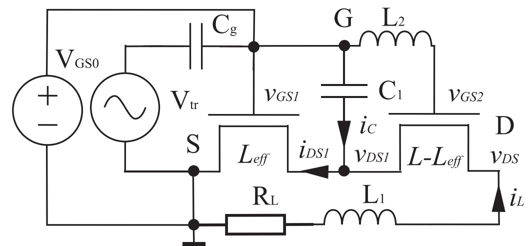

FIG. 7. The scheme of THz detection by FET with load and parasitic elements. S, D, G are the source, drain, and gate terminals of FET THz detector, respectively; R_L is the load resistance of readout circuit, L and L_{eff} are length and effective detection length of transistor channel, respectively, i_L is signal current, V_{tr} is the amplitude of the external THz *ac* voltage, V_{GS0} is the external *dc* bias voltage on gate.

[This article is copyrighted as indicated in the article. Reuse of AIP content is subject to the terms at: http://scitation.aip.org/termsconditions. Downloaded to] IP: 132.199.96.80 On: Fri, 25 Jul 2014 05:14:38

$$i_{DS2} = I_{DS}(v_{DS2}, v_{GS2}, L - L_{eff}), \tag{11a}$$

$$v_{GS2} = V_{GS0}, \tag{11b}$$

$$i_L = i_{DS2}, \tag{11c}$$

$$i_{DS1} = i_{DS2} + i_C. \tag{11d}$$

The value of v_{DS2} is found numerically from equation $I_{DS}\,(v_{DS2}, V_{GS0}, L - L_{eff}) = i_L$.

After averaging Eq. (9) over the period τ and taking into account Eqs. (10a), (10b), (11c), (11d) and $\langle i_C \rangle = 0$, we obtain the equation for i_L current in the read out circuit

$$i_L = \frac{1}{\tau}\int_0^{\tau} I_{DS}[-v_{DS2} - R_L i_L + V_{tr}\cos(\omega t), V_{GS0} + V_{tr}\cos(\omega t), L_{eff}]dt. \tag{12}$$

The photoresponse ΔU is

$$\Delta U = R_L i_L. \tag{13}$$

Equations (11a) and (12) form the system of nonlinear equations with respect to v_{DS2} and i_L. In the case of low radiation intensity ($V_{tr} \ll \varphi_T$, where φ_T is the thermal voltage), Eqs. (11a), (12), and (13) simplifies to Eq. (14a) and ΔU is proportional to $\Im_{ir}$. For large radiation intensities ($V_{tr} \geq \varphi_T$), numerical methods should be used.

For low input intensities, the simple analytical model Eq. (14a) of the broadband photoresponse based on Dyakonov and Shur model[32] was proposed in Ref. 33. It allows calculation of photoresponse using static *I–V* characteristics

$$\Delta U = \frac{V_{tr}^2}{4}\eta_L F_\sigma, \tag{14a}$$

where F_σ is the function of the channel conductivity

$$F_\sigma = \left[\frac{1}{\sigma_{ch}}\frac{d\sigma_{ch}}{dV_{GS}}\right]_{V_{DS}\to 0}, \tag{14b}$$

V_{tr} is the amplitude of the *ac* voltage induced between the gate and source by the THz radiation, V_{GS} is the *dc* voltage between the gate and source, σ_{ch} is the channel conductivity, η_L is the voltage divider transfer coefficient,

$$\eta_L = \frac{1}{1 + R_{ch}/Z_L}, \tag{15a}$$

$$Z_L = \mathrm{R}_L \parallel \frac{1}{j\omega_{\mathrm{m}} C_L}, \tag{15b}$$

where R_{ch} is the channel resistance and Z_L is the complex load impedance of the setup, C_L is the capacitance of measurement circuit, ω_{m} is the modulation frequency. Equation (15a) takes into account that the photoresponse curve depends on the load impedance value of the read-out circuit, since this load impedance forms the voltage-divider with the transistor channel.

The function F_σ in Eq. (14a) is expressed through σ_{ch}, which is useful for processing experimental data. When analytic current expression $I_{DS}(V_{DS}, V_{GS})$ for FET device is known, F_σ in Eq. (14b) can be written as

$$F_\sigma = \left(\frac{\partial I_{DS}}{\partial V_{DS}}\right)^{-1}\frac{\partial^2 I_{DS}}{\partial V_{GS}\partial V_{DS}}. \tag{16}$$

Equation (14a) relates photoresponse value with *dc* characteristics of the transistor. There is no frequency dependency in Eq. (14a) and generally, it should be corrected by introducing the power and frequency dependent factors[27,28] (see Eqs. (4) and (6)).

Previous THz FET models[6,25] used the expression of $I_{DS}(V_{DS}, V_{GS})$ valid either only in the weak inversion or only in the strong inversion regions. Equation (17) is a phenomenological unified equation which describes entire range of transistor operation: strong and weak inversion ranges simultaneously.

Following Ref. 34, we write the drain-source current I_{DS} (V_{DS}, V_{GS}),

$$I_{DS}(V_{DS}, V_{GS}, L) = \frac{W}{L}\mu_n C_{ox}(2\eta)\phi_T^2 \times \left\{\left[\ln(1 + e^{(V_{GS} - V_{th} + \alpha\eta V_{DS})/(2\eta\phi_t)})\right]^2 - \left[\ln(1 + e^{(V_{GS} - V_{th} - \beta\eta V_{DS})/(2\eta\phi_T)})\right]^2\right\}, \tag{17}$$

where W and L are the width and length of transistor channel, respectively; C_{ox} is the gate oxide capacitance per unit area, $\varphi_T = k_B T/q$ is the thermal voltage, k_B is the Boltzmann constant, T is the temperature, q is the electron charge. Equation (17) describes the channel current in all inversion and saturation regions.[34] Equation (17) was used to fit experimental *dc* $I - V$ data in Fig. 4(a) (right ordinate) for HEMT detectors (parameters are presented in Table I). With respect to the original equation in Ref. 34, we add to Eq. (17) terms containing coefficients α and β (in original formula $\alpha = 0$, $\beta = 1$). These fitting parameters allow for better matching with experimental data in the saturation region (slight current increase in Fig. 6(b)). Equation (17) was originally developed for silicon MOSFETs but the one describes HEMT data sufficiently good (see Fig. 6(b)).

The high intensity radiation can result in carriers heating and in heating of the transistor itself. Temperature is one of the main parameters that influence transistor characteristics. It changes characteristics of the transistor and thus changes its intrinsic responsivity. Earlier in Ref. 35, the photoresponse behavior below room temperatures was studied. Here, we consider also the photoresponse behavior for temperatures higher than 300 K. In strong-inversion regime, the channel mobility in FET devices can be written as[34]

$$\mu_n(T) = \mu_n(T_r)\left(\frac{T}{T_r}\right)^{-k_\mu}, \tag{18}$$

where T_r is the temperature at which parameters were extracted and k_μ is the constant temperature coefficient, which varies between 1.2 and 2.[34,36]

[This article is copyrighted as indicated in the article. Reuse of AIP content is subject to the terms at: http://scitation.aip.org/termsconditions. Downloaded to] IP: 132.199.96.80 On: Fri, 25 Jul 2014 05:14:38

The threshold voltage decreases linearly with temperature[34]

$$V_{th}(T) = V_{th}(T_r) - k_{th}(T - T_r), \qquad (19)$$

where k_{th} for Si-MOSFET is between 0.5 and 3 mV/K,[34] for HEMT device k_{th} is smaller for, e.g., 0.3 mV/K.[37] Results of fitting using Eqs. (18) and (19) are presented in Fig. 4(b). One can see good agreement between calculations and experimental data.

To calculate the photoresponse, the following steps are performed: (i) transistor parameters are extracted from *dc* measurements data, (ii) Eq. (12) is numerically solved to get i_L versus incoming irradiation, (iii) ΔU is found using Eq. (13), (iv) comparing experimental and model data in the linear region, the constant k_{ant} is determined and introduced into Eq. (7). The model takes into account the non-linear behavior of the current in the transistor channel. The final fitting results of our model are compared with experimental data in Fig. 6(a). One can see that the model shows good agreement with the experimental data for the MOSFET in all ranges; for HEMT there is a slight deviation from experiment at high intensities. Figure 6(b) shows that the MOSFETs *dc* transfer characteristics are well described by Eq. (17). The accuracy of simulations by model Eq. (17) for HEMT is slightly lower than for MOSFET transistors (Fig. 6(b)). The photoresponse model accuracy depends on the accuracy of the transistor current model.

Performing the simulations with different sets of parameters, we have observed that in principle the non-linear behavior can be also explained by transistor heating by incoming radiation. However we found that reproducing the nonlinear effects in THz FET detectors requires unrealistically high temperatures. Therefore, we can with certainty state that the channel current saturation (similar to one observed in standard *dc* characteristics) is the dominating effect responsible for THz photoresponse saturation at high radiation intensities.

V. CONCLUSIONS

Photoresponse of field effect transistors to THz radiation was observed in a wide range of intensities: from 0.5 mW/cm^2 up to 500 kW/cm^2 and for frequencies from 0.13 THz to 3.3 THz. We demonstrate that photoresponse can be linear with respect to radiation intensity in a wide range of intensities, up to several kW/cm^2. In all cases, we observed that the linear region is followed by the nonlinear part and saturation. Experimental data were successfully interpreted in the frame of the generalized model of THz FET detection. This model takes into account the nonlinear behavior of the channel current in a whole transistor operating range, which is especially important at high THz radiation intensities. Both experiments and theoretical model show that dynamic range of field effect transistors based terahertz detectors extends over many orders of magnitude of intensity of incoming THz radiation.

ACKNOWLEDGMENTS

This work was supported by COST MP1204 "TERAMIR" project and by CNRS-GDR-2987 project "Semiconductor sources and detectors of THz frequencies." We acknowledge also PUF project; DFG (SPP 1459 and GRK 1570), Linkage Grant of IB of BMBF at DLR. We are grateful to M. I. Dyakonov, K. Romanov, and M. Levinshtein for fruitful discussions.

[1]M. I. Dyakonov and M. S. Shur, IEEE Trans. Electron Devices **43**(3), 380–387 (1996).
[2]W. Knap, Y. Deng, S. Rumyantsev, and M. S. Shur, Appl. Phys. Lett. **81**(24), 4637–4639 (2002).
[3]S. Boubanga-Tombet, F. Teppe, D. Coquillat, S. Nadar, N. Dyakonova, H. Videlier, W. Knap, A. Shchepetov, C. Gardes, Y. Roelens, S. Bollaert, D. Seliuta, R. Vadoklis, and G. Valusis, Appl. Phys. Lett. **92**(21), 212101 (2008).
[4]M. I. Dyakonov, Compt. Rend. Phys. **11**(7–8), 413–420 (2010).
[5]W. Knap and M. Dyakonov, in *Handbook of Terahertz Technology*, edited by D. Saeedkia (Woodhead Publishing, Waterloo, Canada, 2013), pp. 121–155.
[6]E. Ojefors, U. R. Pfeiffer, A. Lisauskas, and H. G. Roskos, IEEE J. Sol. State Circ. **44**(7), 1968–1976 (2009).
[7]A. Lisauskas, U. Pfeiffer, E. Ojefors, P. H. Bolivar, D. Glaab, and H. G. Roskos, J. Appl. Phys. **105**(11), 114511 (2009).
[8]D. Perenzoni, M. Perenzoni, L. Gonzo, A. D. Capobianco, and F. Sacchetto, "Optical sensing and detection," Proc. SPIE **7726**, 772618 (2010).
[9]F. Schuster, D. Coquillat, H. Videlier, M. Sakowicz, F. Teppe, L. Dussopt, B. Giffard, T. Skotnicki, and W. Knap, Opt. Express **19**(8), 7827–7832 (2011).
[10]C. Drexler, N. Dyakonova, P. Olbrich, J. Karch, M. Schafberger, K. Karpierz, Y. Mityagin, M. B. Lifshits, F. Teppe, O. Klimenko, Y. M. Meziani, W. Knap, and S. D. Ganichev, J. Appl. Phys. **111**(12), 124504 (2012).
[11]S. Preu, M. Mittendorff, S. Winnerl, H. Lu, A. C. Gossard, and H. B. Weber, Opt. Express **21**(15), 17941–17950 (2013).
[12]K. S. Romanov and M. I. Dyakonov, Appl. Phys. Lett. **102**(15), 153502 (2013).
[13]S. Preu, H. Lu, M. S. Sherwin, and A. C. Gossard, Rev. Sci. Instrum. **83**(5), 053101 (2012).
[14]A. Gutin, V. Kachorovskii, A. Muraviev, and M. Shur, J. Appl. Phys. **112**(1), 014508 (2012).
[15]J. Karch, P. Olbrich, M. Schmalzbauer, C. Zoth, C. Brinsteiner, M. Fehrenbacher, U. Wurstbauer, M. M. Glazov, S. A. Tarasenko, E. L. Ivchenko, D. Weiss, J. Eroms, and S. D. Ganichev, Phys. Rev. Lett. **105**(22), 227402 (2010).
[16]S. D. Ganichev, S. A. Emel'yanov and I. D. Yaroshetskii, Pisma Zh. Eksp. Teor. Fiz. **35**, 297 (1982); JETP Lett. **35**, 368 (1982).
[17]S. D. Ganichev, I. Yassievich, W. Prettl, J. Diener, B. Meyer, and K. Benz, Phys. Rev. Lett. **75**(8), 1590 (1995).
[18]W. Seidel, E. Cizmar, O. Drachenko, M. Helm, M. Justus, U. Lehnert, P. Michel, M. Ozerov, H. Schneider, R. Schurig, D. Stehr, M. Wagner, S. Winnerl, D. Wohlfarth, and S. Zvyagin, in *30th International Free Electron Laser Conference FEL 2008* (Proceedings of FEL, Gyeongju, Korea, 2008), pp. 382–385.
[19]S. D. Ganichev, Y. V. Terentev, and I. D. Yaroshetskii, Pisma Zh. Tekh. Fiz. **11**(1), 46 (1985); Sov. Tech. Phys. Lett. **11**, 20 (1985).
[20]E. Ziemann, S. Ganichev, W. Prettl, I. Yassievich, and V. Perel, J. Appl. Phys. **87**(8), 3843–3849 (2000).
[21]S. D. Ganichev and W. Prettl, *Intense Terahertz Excitation of Semiconductors* (OUP Oxford, UK, 2006), p. 432.
[22]Z.-D. Kvon, S. N. Danilov, N. N. Mikhailov, S. A. Dvoretsky, W. Prettl, and S. D. Ganichev, Phys. E **40**(6), 1885–1887 (2008).
[23]Y. Meziani, J. Łusakowski, W. Knap, N. Dyakonova, F. Teppe, K. Romanjek, M. Ferrier, R. Clerc, G. Ghibaudo, and F. Boeuf, J. Appl. Phys. **96**(10), 5761–5765 (2004).
[24]M. Sakowicz, J. Lusakowski, K. Karpierz, M. Grynberg, W. Knap, and W. Gwarek, J. Appl. Phys. **104**(2), 024519 (2008).
[25]D. But, O. Golenkov, N. Sakhno, F. Sizov, S. Korinets, J. Gumenjuk-Sichevska, V. Reva, and S. Bunchuk, J. Semicond. **46**(5), 678–683 (2012); Fiz. Tek. Polupr. **46**(5), 965-700 (2012).
[26]A. J. Kreisler, Proc. SPIE **0666**, 51 (1986).
[27]S. Boppel, A. Lisauskas, M. Mundt, D. Seliuta, L. Minkevicius, I. Kasalynas, G. Valusis, M. Mittendorff, S. Winnerl, V. Krozer, and H. G.

[This article is copyrighted as indicated in the article. Reuse of AIP content is subject to the terms at: http://scitation.aip.org/termsconditions. Downloaded to] IP: 132.199.96.80 On: Fri, 25 Jul 2014 05:14:38

Roskos, IEEE Trans. Microwave Theory Technol. **60**(12), 3834–3843 (2012).
[28]M. Sakhno, F. Sizov, and A. Golenkov, J. Infrared Millimeter Terahertz Waves **34**(12), 798–814 (2013).
[29]C. A. Balanis, *Antenna Theory: Analysis and Design*, 3rd ed. (John Wiley & Sons, New Jersey, 2005), p. 1136.
[30]V. Y. Kachorovskii, S. L. Rumyantsev, W. Knap, and M. Shur, Appl. Phys. Lett. **102**(22), 223505 (2013).
[31]W. Knap, M. Dyakonov, D. Coquillat, F. Teppe, N. Dyakonova, J. Łusakowski, K. Karpierz, M. Sakowicz, G. Valusis, D. Seliuta, I. Kasalynas, A. Fatimy, Y. M. Meziani, and T. Otsuji, J. Infrared Millimeter Terahertz Waves **30**(12), 1319–1337 (2009).
[32]M. I. Dyakonov and M. S. Shur, IEEE Trans. Electron Devices **43**(10), 1640–1645 (1996).
[33]M. Sakowicz, M. B. Lifshits, O. A. Klimenko, F. Schuster, D. Coquillat, F. Teppe, and W. Knap, J. Appl. Phys. **110**(5), 054512 (2011).
[34]Y. Tsividis and C. McAndrew, *Operation and Modeling of the MOS Transistor* (Oxford University Press, New York, 1999), p. 620.
[35]O. A. Klimenko, W. Knap, B. Iniguez, D. Coquillat, Y. A. Mityagin, F. Teppe, N. Dyakonova, H. Videlier, D. But, F. Lime, J. Marczewski, and K. Kucharski, J. Appl. Phys. **112**(1), 014506 (2012).
[36]S. Vitanov, V. Palankovski, S. Maroldt, and R. Quay, Solid State Electron. **54**(10), 1105–1112 (2010).
[37]M. Ni, P. Fay, and N. Pan, in *Proceedings of the International Conference on Compound Semiconductor Manufacturing Technology, CS Technology Conference, 24-27 April, 2006* (CS MANTECH, Vancouver, British Columbia, Canada, 2006), pp. 247–250.

[This article is copyrighted as indicated in the article. Reuse of AIP content is subject to the terms at: http://scitation.aip.org/termsconditions. Downloaded to] IP: 132.199.96.80 On: Fri, 25 Jul 2014 05:14:38